Canadian Journal of Forest Research

Article

Carbon and biomass models for five Sierra Nevada mixed conifer species

Dryw A. Jones[a] **and Kevin L. O'Hara**[b]

[a]Research Forester for USDA Forest Service Pacific Northwest Research Station, 3625 93rd Avenue SW Olympia, WA 98512, USA; [b]Retired Professor of Silviculture University of California at Berkeley, 130 Mulford Hall Berkeley, CA 94720, USA

Corresponding author: **Dryw Jones** (email: dryw.jones@usda.gov)

Abstract

Data from tree cores and disks were used to develop biomass and carbon mass taper models for five major Sierra Nevada conifer species. These taper models were used to predict masses of tree boles, tree bole portions, branch, and foliage using carbon fraction data for oven-dried and living tissues. Taper models developed using core data were well modeled to disk data with R^2 values ranging from 0.98 to 0.99 by inclusion of a calibration parameter. The fit of the final models suggests our approach can be used to include large diameter trees that cannot be cut down in biomass data collection efforts that otherwise would only sample smaller diameter trees. Our results show that biomass-weighted living carbon estimates at the whole tree level ranged from 2.8% to 9% higher than estimation methods using the standard carbon fraction of 0.5 depending on the tree species. Our approach addresses the need to account for variation in carbon fraction and wood density throughout trees, as well as demonstrating a data collection and modeling approach to include large old growth trees that cannot be destructively sampled.

Key words: Sierra Nevada conifers, taper model, biomass, carbon fraction, wood density

Introduction

Globally carbon mass estimates are an increasingly important part of land management and are critical to understanding carbon dynamics within ecosystems. Carbon flux from management activities, or natural disturbances, is significantly influenced by the total carbon in a given site (Hoover and Stout 2007). In addition to total carbon mass, the distribution of that carbon within an ecosystem can also influence carbon flux due to different decay rates within carbon pools (Cousins et al. 2015), or different types of disturbance (Hoover and Stout 2007; Eskelson et al. 2016). Accurate estimates of carbon flux therefore require accurate estimates of the amount of carbon stored in ecosystems including large pools of carbon contained within forests. Without these accurate estimates, land management designed to sequester carbon may not meet its objectives.

Current carbon estimation approaches commonly convert volume estimates to biomass using species average wood density values and a universal carbon fraction conversion factor of 0.5 (e.g., Woodall et al. 2011). The 0.5 value likely comes from research devoted to global estimates of carbon mass which suggest a global average value near 0.5 (e.g., Ajtay et al. 1979), though there is no indication that this value was ever validated at that scale (Lamlom and Savidge 2003; Thomas and Martin 2012). This 0.5 carbon conversion factor, or carbon fraction, is commonly used in studies that estimate forest carbon at smaller scales as well (e.g., Cohen et al. 1996; Goodale et al. 2002; Chave et al. 2005; Woodbury et al. 2007; Fahey et al. 2009; Lutz et al. 2017). Carbon fractions have been shown to vary significantly between tree species and within individual trees (Lamlom and Savidge 2003, 2006; Thomas and Martin 2012; Jones and O'Hara 2012, 2016). Therefore, using measured carbon fractions improves the accuracy and precision of carbon mass estimates of trees and forests.

In addition to improving carbon mass estimates by using measured carbon fractions, there can be significant improvements in carbon mass estimates of living tissues by using analytic methods that most accurately capture volatile organic compounds (Jones and O'Hara 2016). The majority of measured carbon fractions underestimate the carbon fractions of living tissues by failing to capture the volatile carbon contained in living tissues (Lamlom and Savidge 2003; Thomas and Martin 2012; Jones and O'Hara 2016). Accurately measuring living carbon fractions inclusive of the volatile component and applying those fractions to their respective tissue type biomasses will therefore improve the accuracy of carbon estimates of living plants.

Biomass models using average wood density values are used for several species across many regions (Woodall et al. 2011). The application of these models is most suitable for biomass estimates across a species range, as wood density can vary significantly across the species range (Chave et al. 2009; Jones and O'Hara 2012). Wood density can also vary within tree boles (Rueda and Williamson 1992; Woodcock and Shier

2002; Ver Planck and MacFarlane 2014), across tree ring ages and growth rates (Langum et al. 2009), and significantly vary by tree height (Zhao et al. 2016). Therefore, the accuracy of biomass estimates would improve if this variation was accounted for in biomass models, rather than utilizing a species average value.

The combined effect of deviations in wood density from the species average, and carbon fractions from the 0.5 value, can result in underestimates of carbon mass of as much as 16% in coast redwood (*Sequoia sempervirens* (D Don) Endl.) tree boles (Jones and O'Hara 2012). Overestimates are also likely given the lower than 50% measured carbon fraction in many hardwoods (Lamlom and Savidge 2003; Thomas and Malczewski 2007; Thomas and Martin 2012). These inaccuracies can be addressed by accounting for changes in wood density and carbon fraction related to easily measured tree characteristics (Jones and O'Hara 2016, 2012). Developing carbon mass prediction models that account for variation in wood density and carbon fraction utilizing commonly collected tree characteristics would be a significant step in improving carbon mass estimates.

Although whole tree biomass equations have been developed for several species (Chojnacky et al. 2014), we are unaware of any carbon mass prediction equations that have been developed that capture all of the previously mentioned sources of variation in carbon fraction within trees, and between tree components. Additionally large diameter trees are often not included in allometric models for a given species resulting in the use of proxy species models (Lutz et al. 2017), or extending the allometric model past the diameter range it was fit to. To improve carbon mass estimation in forests, it is therefore necessary to develop models that accurately account for the variation in wood density and carbon fraction between tree species and within individual trees. Converting existing biomass models to carbon models with an appropriately weighted carbon fraction could achieve this result; however, this approach risks ignoring covariance between carbon fraction and wood density (Jones and O'Hara 2018).

Biomass models that predict biomass and biomass distributions exist (Jordan et al. 2006; Zakrzewski and Duchesne 2012; Ver Planck and MacFarlane 2014). These models have the advantage of estimating biomass for standing trees and harvested logs using the same equation, thereby allowing tracking of stand-level biomass in logs removed, as well as in the portion of the bole remaining on site during harvest operations, which is useful for carbon accounting. A model that connects this biomass estimation flexibility while also accurately capturing the variation in carbon fraction would allow for easier tracking of carbon mass between harvests and would be a valuable tool in the study of carbon dynamics at the stand to ecosystem scales.

Branch and bark biomass have not been studied to the same degree as bole biomass, but are strongly correlated with bole biomass (Chojnacky et al. 2014). Given this strong biomass relationship, it is likely that branch and bark carbon masses are also strongly correlated with bole carbon masses; however, accounting for carbon fraction of tissues is necessary to determine exactly what that correlation might be (Elias and Potvin 2003; de Aza et al. 2011; Jones and O'Hara 2016).

A significant amount of biomass research has focused on accurately estimating wood volume (Brown 2002; Woodall et al. 2011; Chojnacky et al. 2014). There is a very good reason for this, as tree volume drives overall biomass and carbon mass predictions. As wood volume is typically the most important economic consideration in forest management, accounting for total volume in biomass and carbon mass prediction models, in addition to capturing carbon fraction and wood density variation, would be ideal. One approach to capturing variation in these three tree properties is a modified form of the density-integral method described by (Parresol and Thomas 1989). This approach can capture the variation in wood density and carbon density to yield accurate predictions of biomass, or carbon mass, for the entire tree bole and bole portions by integrating biomass and carbon mass taper models.

To address the need for carbon and biomass estimation models that account for known sources of variation within trees and tree components, we developed carbon and biomass taper models for important conifer species from the Sierra Nevada, a region with large amounts of carbon storage (Mattson and Zhang 2019), fit to a range of diameters with these specific objectives in mind: (1) develop biomass and carbon mass models for whole tree, tree bole, bark, branch, and foliage components using a calibrated density-integral method for ecologically and economically important tree species; and (2) compare the resulting model estimates to "standard" methods to determine any improvement in predictive power of the new approach.

Methods and materials

Plot locations

Five ecologically and economically important conifer tree species from the mixed conifer forest type of the Sierra Nevada were sampled: sugar pine (*Pinus lambertiana* Dougl.), ponderosa pine (*P. ponderosa* Lawson & C. Lawson), coast Douglas-fir (*Pseudotsuga menziesii* (Mirb.) Franco var. *menziesii*), white fir (*Abies concolor* (Gord. & Glend.) Lindl. ex Hildebr.), and incense-cedar (*Calocedrus decurrens* (Torr.) Florin). Trees were sampled across a latitudinal range in the Sierra Nevada at the following locations: (1) Baker Forest (39.916N, 121.063W), (2) Blodgett Research Forest Station (38.910N, 120.662W), and (3) near Shaver Lake, CA (37.046N, 119.211W). Table 1 shows summary statistics for sample trees and sample sizes.

Tissue sample collection and processing

Sample trees were stratified by 10 cm diameter classes and randomly selected within sites for each species present. This resulted in samples that represent tree sizes from very young to old growth (>400 years). Tree diameter at breast height (1.37 m) ranged from 6.0 to 155.1 cm for Douglas-fir, 4.4–108.3 cm for incense cedar, 12.9–142.5 cm for ponderosa pine, 5.0–195.7 cm for sugar pine, and 5.49–112.6 cm for white fir. Tree heights ranged from 4.2 to 60.0 m for Douglas-fir, 2.3–46.8 m for incense cedar, 8.3–60.0 cm for

Table 1. Sample summary data for wood density, carbon fraction, tree cores, and tree disks.

Species	Tree disk data				Tree core data		Wood density			Carbon fraction		
	DBH (cm)	Height (m)	*n*—tree	*n*—disk	DBH (cm)	Height (cm)	*n*—trees	*n*—cores	*n*—segments	*n*—trees	*n*—cores	*n*—segments
Douglas-fir	15.9 (7.0)	11.9 (5.7)	5	24	61.2 (31.7)	35.1 (9.6)	14	47	565	4	6	24
Incense-cedar	14.2 (8.2)	7.2 (3.6)	6	17	48.1 (32.0)	22.26 (11.8)	15	51	759	7	9	24
Ponderosa pine	18.1 (3.9)	12.8 (5.0)	6	25	71.8 (37.6)	35.4 (13.6)	16	47	950	6	8	40
Sugar pine	18.4 (11.1)	11.6 (6.8)	7	39	95.5 (47.4)	40.0 (11.6)	14	55	891	6	8	23
White fir	15.8 (10.4)	10.6 (6.7)	7	36	57.7 (26.8)	31.4 (9.3)	27	76	1009	5	10	32

Notes: Diameter at breast height (DBH), total tree height (Height), and number of samples (*n*) are indicated for each species. For DBH and height, the mean value is followed by the standard deviation in parenthesis. Sample size for trees and disks or cores, as well as density and carbon fraction sample size, are shown for tree disks and tree cores.

ponderosa pine, 3.8–66.7 cm for sugar pine, and 4.1–51.5 cm for white fir. Tree cores were taken from different heights within each tree. Height to core, bole diameter, and bark thickness were recorded for each core taken. Sample trees were either climbed if safe to do so or cut down. Cores were taken at breast height (1.37 m), base of live crown (HLC), and every 4 m within the live crown for each tree. A 400 mm long Haglöf increment borer, with an aperture of 5.15 mm, was used to extract cores. Cores were placed in clear plastic straws, sealed using adhesive tape, labeled, and placed in a rigid white plastic tube. Core sapwood boundaries were determined in the field by marking the boundary of the translucent section of the cores on the outside of the straws. Cores were placed in a cooler and transported back to the lab. In the lab, cores were placed in a freezer maintained between −24 °C and −18 °C. A total of 276 cores from 86 trees were processed for wood density. Wood density cores were separated into bark and wood segments containing four growth rings until the entire core was processed. If the innermost core segment contained fewer than four growth rings, the segments lengths were measured and the number of rings recorded. A total of 41 cores were analyzed for carbon fractions. These cores were separated into tissue types (bark, sapwood, and heartwood) for carbon fraction analysis. A more complete description of this process can be found in Jones and O'Hara (2016).

Branch and foliage sampling

Within the crown of each tree, two branches were randomly selected from each third of the crown, for a total of six branches per tree and a total of 360 branches for the study. Sampled branches and all other branches along the bole were measured starting at the base of live crown to the tip of the tree for felled trees, and to the highest point climbed on trees that were not cut down. All branch diameters were measured above the branch collar on the major and minor axis using calipers with a precision of 0.5 mm. Branch height from the ground was recorded to the nearest cm using 15 m logger tape (Spencer model 950MER) secured at breast height on the bole. When the limit of the tape was reached, it was reattached to a known height and that height was recorded to adjust additional height measurements to the new base height. Foliage was separated from the branch in the field and branches were cut, weighed, and placed in bags then labeled with tree ID and branch ID. In the lab, branches were placed in paper bags, labeled and oven dried at 103 °C until weights stabilized, at which point their weights were recorded. Branch carbon mass was calculated by multiplying total branch biomass by the average carbon fractions of the whole bole. Average bole carbon fractions were derived by multiplying the proportion of bole mass in heartwood, sapwood, and bark by their respective carbon fractions and summing the results. This approach assumes s typical 1:1 relationship between branch and bole carbon (Thomas and Martin 2012).

Proportional foliage subsamples were collected from each needle age class present in each sample branch and placed in a small plastic resealable bag, and then labeled with tree

Table 2. Oven-dry and living carbon fraction data by tissue type.

Carbon type	Species	Bark	Heartwood	Sapwood	Foliage
Oven-dry	Douglas-fir	0.569 (0.009)	0.501 (0.005)	0.498 (0.001)	0.515 (0.004)
	Incense-cedar	0.553 (0.03)	0.531 (0.009)	0.509 (0.008)	0.513 (0.004)
	Ponderosa pine	0.523 (0.008)	0.514 (0.009)	0.499 (0.009)	0.510 (0.005)
	Sugar pine	0.563 (0.007)	0.521 (0.005)	0.516 (0.002)	0.509 (0.002)
	White fir	0.493 (0.002)	0.488 (0.002)	0.494 (0.002)	0.521 (0.003)
Living	Douglas-fir	0.588 (0.009)	0.503 (0.01)	0.51 (0.009)	0.518 (0.006)
	Incense-cedar	0.567 (0.015)	0.545 (0.009)	0.541 (0.008)	0.517 (0.007)
	Ponderosa pine	0.528 (0.008)	0.527 (0.008)	0.512 (0.005)	0.522 (0.006)
	Sugar pine	0.57 (0.01)	0.534 (0.005)	0.532 (0.009)	0.517 (0.002)
	White fir	0.525 (0.01)	0.517 (0.004)	0.507 (0.009)	0.52 (0.001)

Notes: Mean carbon fractions for four tissue types from five conifer species shown. Standard deviations are shown in parenthesis next to the mean value for each category. Carbon fraction is the mass of carbon per unit mass of material adjusted to oven-dry moisture content. Data are derived from work performed by Jones & O'Hara (2016).

ID and branch ID. Foliage sample bags were placed on ice in the field for transport, and then placed in a freezer in the lab. Foliage was weighed in the lab after drying in a force air oven at 101 °C for 24 h. A more detailed review of the leaf sampling can be found in Jones et al. (2015). Twelve foliage samples were randomly selected for carbon fraction analysis from eight different trees, representing five tree species. A total of 360 branch foliage samples were collected and used for modeling individual branch foliage masses.

Core segment density and carbon density

Wood density core segments were measured for length using digital calipers with a precision of 0.001 cm. The volume of each segment was calculated by multiplying segment length (in the green state) by the area of the increment borer aperture (0.832 cm^2). Wood density segments were then wrapped in aluminum foil labeled with a unique core ID and segment ring numbers, and then oven-dried at 103 °C until weights stabilized. Stable mass of the density segments was recorded and divided by the core segment volume resulting in core segment density (D) values in $g \cdot cm^{-3}$.

This study uses carbon fractions (CF) measured by oven-dry methods and the minimized loss of carbon (MLC) method described in Jones and O'Hara (2016). Oven-dry methods best estimate kiln dried timber, while the MLC method is a better representation of living tissue carbon (Jones and O'Hara 2016). Mean carbon fraction values are given for each species tissue type in Table 2. Carbon mass for each carbon sample was determined using a CE Instruments Flash 2000 CHNS/O analyzer, which was calibrated between runs of 40 samples using acetanilide as the standard. Standards were also placed every tenth sample to ensure calibration accuracy. Carbon mass was divided by oven-dry sample mass to adjust all carbon fractions to the same baseline moisture content. This process resulted in carbon fractions for living tissues and oven-dry tissues as shown in Table 2. The tissue specific oven-dry and MLC carbon fractions were multiplied by individual segment densities to yield carbon densities (CD) in units of grams carbon/cm^3 for each segment.

Linear density (mass per unit tree height in $g \cdot cm^{-1}$) for cores was calculated as the sum of core wood segment area densities (density of segment times area of toroid represented by segment) shown in Fig. 1 from the pith to the outermost wood portion (see Supplementary material for more detail), for biomass, oven-dry carbon mass, and living carbon masses. Representative segment toroid areas were determined as the difference between the bole area represented by the outside of the core segment minus the bole area represented by the inside of the core segment. Linear density in this study represents the mass of wood in a tree bole disk that is 1 cm high with a density equal to the area-weighted densities of the sampled tree core segments (Fig. 1).

Disk biomass and carbon mass

Table 1 shows summary statistics for the tree disk data that were used to calibrate models developed from core data to account for any compression, or expansion of extracted core tissue, along with summary data for samples used to develop linear density data from tree cores. Sample disks were removed from felled trees using a chainsaw at heights of 0.3 m, 1.37 m, halfway between 1.37 m and live crown, live crown, and every 2 m within the live crown. Each disk was labeled with a unique tree ID, and disk height along the bole. Disks were placed in paper bags with bark attached and sealed with adhesive tape and then labeled with tree ID and disk height. In the lab, disks were measured for thickness using digital calipers at four locations on the disk, starting with the tallest portion of the disk, and at increments of 90° around the disk. The average of these measurements (disk thickness) was used to determine the height of the bottom and top of the tree disk from the ground prior to the tree being cut down using markings on the bark as reference points. Once measured, disks with bark still attached were placed back into labeled paper bags and placed in an oven set to 103 °C, and dried until weight stabilized. Total disk masses were recorded using an Ohaus Analytical Plus balance (model AP310), with bark masses determined by subtracting the mass of the disk with bark removed from the total disk mass.

Tree disks were photographed in the field with a ruler placed on them for reference. These photographs were used to determine the ratio of heartwood to sapwood present in the tree disks after marking the sapwood/heartwood

Fig. 1. Visual representation of linear density, core segment area density, and area density. Area density is calculated by multiplying core density times the circumference represented by the distance from pith to core segment center. Linear density is the sum of these area densities to a given radius yielding the mass of a 1 cm tall section of the tree bole at a given height.

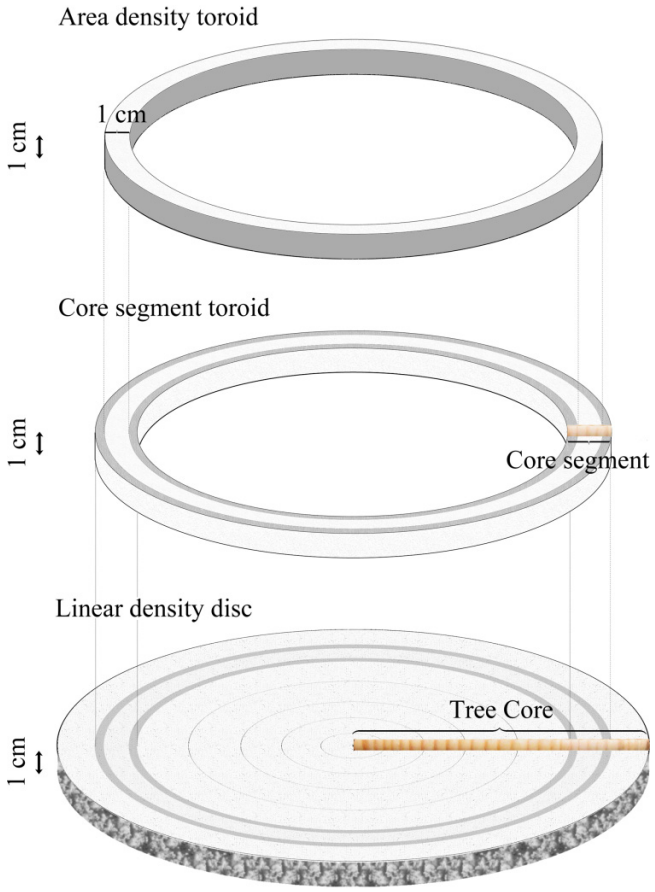

boundary in the field with a black permanent marker. Disk carbon mass was calculated by multiplying disk biomass by the weighted carbon fraction determined by the ratio of heartwood to sapwood area. This calculation was performed for both living carbon and oven-dry carbon estimates.

Statistical analysis

We used nonlinear mixed effects (NLME) methods to model all mass relationships, as they are well suited to the grouped data collected for the study. The modeling approach allows for the application of fixed effect parameter estimates for population-level variables of interest such as live crown ratio, or species, and random effect parameter estimates for grouping levels, such as core within tree, and tree within site where variation is naturally expected to occur without generalizable application to the population of interest. Random effects are assumed to be normally distributed with a mean of zero. The approach is effective in modeling within-group correlations and can handle the unbalanced data set we have in this study (Pinheiro et al. 2019). All analyses were performed using the NLME package (version 3.1–118) (Pinheiro et al. 2015) in the R statistical platform (R Development Core Team 2015). All models were initially fit with maximum likelihood regression methods when model comparisons were made, but all final models indicated in Table 3 were fit with restricted maximum likelihood methods to derive final parameter estimates. Where necessary, different variance structures were tested until normality of residuals and random effects was achieved. As part of the modeling process, additional covariates were added to model parameters to test for significantly improved model fit. This process effectively replaced a parameter with a parameter matrix containing covariates of interest and new parameters to be fit. For example, parameter α_s in Model 8 (Table 3) would become ($\alpha_s + \alpha_1$*RH) to test if relative height significantly improved the model. All covariates that are used in the initial models, along with their descriptions can be found in Table 3; any additional covariates determined to significantly improve model fit are found in associated parameter estimate tables for the final model fits.

Bole area density and area carbon density were modeled using NLME models (Pinheiro et al. 2015). Table 3 shows the initial model forms that were evaluated for fit to bole area density data. Model forms for each category were chosen by testing different model forms against each other after graphical analysis of the data to determine a general pattern. The best model for each tree characteristic was determined by log-likelihood ratio testing of models fit using maximum log-likelihood approaches (Pinheiro et al. 2015), including an evaluation of model AIC and BIC. The NLME package uses the log of the likelihood statistic to handle precision limits on most computers while providing the same utility of the likelihood statistic. Final model parameters were estimated using restricted maximum log-likelihood regression as this approach generally results in less biased parameter estimates. Random effects were assigned to cores (i) nested within tree (j) for models 1–6 in Table 3. For models 8 and 11, random effects were assigned at the individual tree (j) level. If random effects for any parameter were not significantly different from zero, they were dropped. Sample sizes for area density models are shown for each species in Table 1 under the wood density *n*-segment column.

To estimate the missing portion of linear density in cores that did not reach the pith, the best-fitting model for area density was integrated from zero to the radius of the missing portion of the core. This value was added to the sum of representative linear densities for the rest of the core resulting in total core wood linear density.

Linear density was modeled throughout the tree bole using a taper function (Model 7; Table 3) that was originally developed to predict radial bole taper of the species in this study, and performed better than other taper functions it was compared to (Biging 1984). This model form has logical assumptions that apply equally well to linear density as they do to tree radial profiles. Those assumptions are that the taper at the base of the tree has the largest value and values are progressively lower at every point above the base, and any values above the top of the tree should be equal to zero. The model form was fit to linear density data without the addition of any other covariates to create a simpler model form that would be

Table 3. Model forms by tree portion and characteristics modeled.

Tree portion	Model no.	Model form	DF
Bole	1	$B_a = (\alpha_s + \alpha_{ij}) * r * e^{-e^{\frac{-DT^{\beta_s+\beta_{ij}}}{HLC}}} + \varphi_{ij}$	4158
	2	$B_a = (\alpha_s + \alpha_{ij}) * r * e^{-e^{\frac{-DT^{\beta_s+\beta_{ij}}}{HT}}} + \varphi_{ij}$	
	3	$B_a = (\alpha_s + \alpha_{ij}) * r * \left(1 - e^{-(\beta_s+\beta_{ij})*\frac{DT^{\theta_s+\theta_{ij}}}{HLC}}\right) + \varphi_{ij}$	
	4	$B_a = (\alpha_s + \alpha_{ij}) * r * \left(1 - e^{-(\beta_s+\beta_{ij})*\frac{DT^{\theta_s+\theta_{ij}}}{HT}}\right) + \varphi_{ij}$	
	5*	$B_a = (\alpha_s + \alpha_{ij}) * r * e^{\frac{(\beta_s+\beta_{ij})*DT}{HT}} * e^{\frac{-(\theta_s+\theta_{ij})*e^{\left((\beta_s+\beta_{ij})*\frac{DT}{HT}-1\right)}}{(\beta_s+\beta_{ij})}} + \varphi_{ij}$	
	6	$B_a = (\alpha_s + \alpha_{ij}) * r + \varphi_{ij}$	
Bole linear density	7	$B_l = \pi * \left(\mathrm{DBH} * \left(\alpha_s + \beta_s * \ln\left(1 - \left(1 - e^{-\frac{\alpha_s}{\beta_s}}\right) * \left(\frac{HT_c}{HT}\right)^{\frac{1}{3}}\right)\right)\right)^2$	266
Branch	8	$BR_m = (\alpha_s + \alpha_j) * A_{br} * RD^{\beta_s+\beta_j-1} * e^{-RD^{\beta_s+\beta_j}} + \varphi_j$	341
	9	$BR_{tm} = \alpha_s * DBH^{\beta_s} * e^{\theta_s * CL}$	37
Bark	10	$BRK_m = \alpha_s * M_{dw}$	134
Foliage	11	$F_m = (\alpha_s + \alpha_j) * A_{br} * RD^{\beta_s+\beta_j-1} * e^{-RD^{\beta_s+\beta_j}} + \varphi_j$	341
	12	$F_{tm} = DBH^{\beta_s} * e^{\theta * CL}$	37
Bole	13	$B_{lc} = \mathrm{CS} * \text{Model 7}$	134

Notes: Model forms fit to data for the respective tree portion are shown above. For mixed effects models, the random effects are normally distributed with a mean of 0. Models 1 through 6 were compared directly for performance in predicting bole area densities and the best-fitting model was determined using log-likelihood ratio testing. DT (m) is the distance from the top of the tree, HLC (m) is the height from the ground to the lowest live branch, HT is the total tree height (m), CL (M) is the length of live crown, r (cm) is the radius to the center of the core segment, DBH is the diameter of sample trees at 1.37 m from the ground, HT_c is the distance from the ground to sample core (m), RD is relative depth in the crown, A_{br} is the cross-sectional area of a branch, and M_{dw} is the wood mass of disks taken from sample trees, B_a is bole area density, B_l is bole linear density of cores, BR_m is individual branch mass, BR_{tm} is whole tree branch mass, BRK_m is bark mass of bole disks, F_m is individual branch foliage mass, F_{tm} is whole tree foliage mass, and B_{lc} is the calibrated bole wood mass. α_s, β_s, and θ_s are parameters to be estimated by species and φ_i or φ_{ij} are the normally distributed within group error terms for the given levels of grouping. Random effects grouping for a given parameter are indicated with subscripts i and j, with i representing the cores grouping level and j representing the individual tree grouping. C_S is the calibration parameter determined by fitting area mass data to disk mass data by species. * Indicates that Model 5 with additional covariates fit the data best. DF is the minimum degrees of freedom for each model group, defined as the number of observations used to fit the model minus the number of parameters estimated in the model.

easier to incorporate into existing estimation procedures for whole tree bole biomass, and carbon mass. Sample sizes for linear density modeling are shown for each species in Table 1 under the wood density *n*-cores column.

Bark mass was modeled as a fraction of disk wood mass using linear regression to fit Model 10 (Table 3) to data from tree disks. Foliar mass and branch mass were modeled at the individual branch level by fitting the respective models in Table 3—the data. These individual branch models were then applied to trees in which all branches had been measured for branch height along bole and branch diameter. The resulting branch and foliage masses were summed for the whole tree for felled trees. These whole tree masses were used to model the whole tree foliage and branch masses by fitting the appropriate models from Table 3—the whole tree data. Sample sizes for bark mass estimates are shown for each species in Table 1 under the tree disk data *n*-disk column.

For the best-fitting model of area density, individual branch, and foliage branch mass, conditional (R_c^2) and marginal (R_m^2) values were calculated following the procedures in Nakagawa and Schielzeth (2013). The R_c^2 values represent the portion of variance explained by the entire model including random effects, while the R_m^2 values represent the proportion of variance explained by the modeled fixed effects only. Standard errors are presented in parenthesis following all mean values except for Tables 1 and 2, where standard deviations are shown in parenthesis.

Biomass and carbon mass estimation comparisons

To determine differences in mass proportions, and total tissue masses, the final biomass models for foliage, branch, bark, and bole tissues were compared to models using a "standard" approach to biomass and carbon mass estimation called the component ratio method (CRM) (Woodall et al. 2011). To account for model selection error in biomass estimates (Melson and Harmon 2011), example trees were all set to a total biomass of 1000 kg. For the CRM estimation approach, branch and treetop, bole, bark, and foliage were estimated using equations in Woodall et al. (2011), as they are well-established in carbon accounting protocols and can predict most of the tissue types presented in this paper. To get separate mass estimates for branch and bole, we calculated the ratio of mass in treetop relative to merchantable stem mass using Model 7 integrated from base to a height where bole wood diameter is 10.16, the merchantable top definition from Woodall et al. (2011), and then from merchantable top to treetop. Height to this diameter was determined by

Table 4. Parameter estimates for the linear density models fit by species and density type.

Linear density type	Species	α_s	β_s	C_s
Biomass	Douglas-fir	0.363 (0.01)	0.15 (0.014)	1.07 (.03)
	Incense-cedar	0.309 (0.01)	0.119 (0.012)	1.32 (0.03)
	Ponderosa pine	0.356 (0.01)	0.149 (0.018)	1.02 (.03)
	Sugar pine	0.331 (0.006)	0.114 (0.007)	1.04 (.02)
	White fir	0.327 (0.007)	0.122 (0.011)	1.16 (.02)
Oven-dry carbon	Douglas-fir	0.256 (0.007)	0.106 (0.01)	1.07 (.03)
	Incense-cedar	0.219 (0.007)	0.081 (0.008)	1.34 (0.04)
	Ponderosa pine	0.252 (0.007)	0.104 (0.013)	1.02 (.03)
	Sugar pine	0.238 (0.004)	0.082 (0.005)	1.03 (.01)
	White fir	0.229 (0.005)	0.085 (0.008)	1.17 (.02)
Living carbon	Douglas-fir	0.259 (0.007)	0.107 (0.01)	1.07 (.03)
	Incense-cedar	0.228 (0.007)	0.087 (0.009)	1.32 (0.03)
	Ponderosa pine	0.256 (0.007)	0.107 (0.013)	1.02 (.03)
	Sugar pine	0.242 (0.004)	0.084 (0.005)	1.04 (.02)
	White fir	0.234 (0.005)	0.087 (0.008)	1.16 (.02)

Notes: Mean parameter estimates followed by standard error of the estimate in parenthesis are shown for biomass, living carbon, and oven-dry carbon linear density models for five species. Parameter estimates α_s and β_s are for Model 7 in Table 3, while the C_s parameter estimate is for Model 13.

setting Model 7 (Table 3) equal to 10.16 and solving for the root of the function using the package rootSolve (Soetaert 2009) in the R statistical software platform (R Development Core Team 2015). Top mass was then allocated to bark and bole assuming the same proportions as found in the CRM estimates to yield separate stem and branch masses. To ensure representative tree dimensions, the average height-to-diameter ratio for the trees in this study for each species were used to confine example tree heights to a proportion of a given diameter. Tree diameter was then set for each species so that the total estimated biomass of each example tree was equal to 1000 kg using the whole tree biomass models mentioned above. To obtain heartwood and sapwood mass values for study estimates, the average heartwood to inside bark area density ratio was determined from tree cores and then applied to the total bole wood mass estimate obtained from integrating Model 7 from 0 to the top of the tree. Sapwood mass was then determined by subtracting heartwood mass from bole mass. Bark mass was obtained using Model 10 (Table 3) with stem wood mass estimates in place of M_{dw}.

Results

Linear density

The mean and standard deviation for the percentage of linear density in the missing portion of all cores was 3.7 (7.9)%. Given the importance of including large trees in the data set, it was deemed necessary to estimate the missing portion of linear density by numerically integrating Model 5 from the pith to the estimated radius of the missing portion of the core. The full linear density data set was used to estimate parameters for Model 7 (Table 3), with the resulting linear density parameter values shown in Table 4.

The best-fitting models had significantly different parameter estimates for α_s and β_s between species demonstrating significant differences in carbon mass distributions along tree boles. For example, Douglas-fir has the highest α_s and the highest β_s values. High α_s values indicate that the proportion of mass at the base of the tree relative to the mass at DBH is higher than for other species suggesting increasing density toward the stump. This trend is enhanced by the higher β_s values that indicate greater mass taper translating to a greater distribution of mass to the base of the tree. The relative ranking of parameter estimates between species does not change across mass types (biomass, oven-dry, and living carbon), suggesting that much of the variation in mass distributions is driven by differences in wood density and less so by carbon fraction.

Disk mass predictions

Estimates from Model 7 showed good fit to the observed values (Fig. 2). The overall fit of the models was very good with measured R^2 values in the range of 0.94 to 0.99 depending on species. Most species demonstrated an even spread around the one-to-one line in Fig. 2, indicating the models account for the variation in the data across the range of predicted values and tree sizes. There does appear to be a slight deviation from the one-to-one line in the incense-cedar data near the middle of the data range. This deviation, however, does not appear to impact the predicted disk wood mass values shown in Fig. 3.

The predicted disk wood mass estimates were derived through numerical integration of Model 7, using parameters from Table 4. The integration range was from height above the ground from the bottom of the individual tree disks to the top of the disks. The fit of the data shown in Fig. 3 is very good, with the lowest R^2 value being 0.98. There is divergence from a one-to-one relationship with slopes (C_S estimates for Model 13; Table 3) between 1.02 and 1.32 depending on species, indicating that disk wood mass predictions

Fig. 2. Observed linear density compared to predicted linear density. The black line in each graph represents the one-to-one line where predictions equal observed values. R^2 values represent the proportion of variance captured by the respective models for each species and mass type.

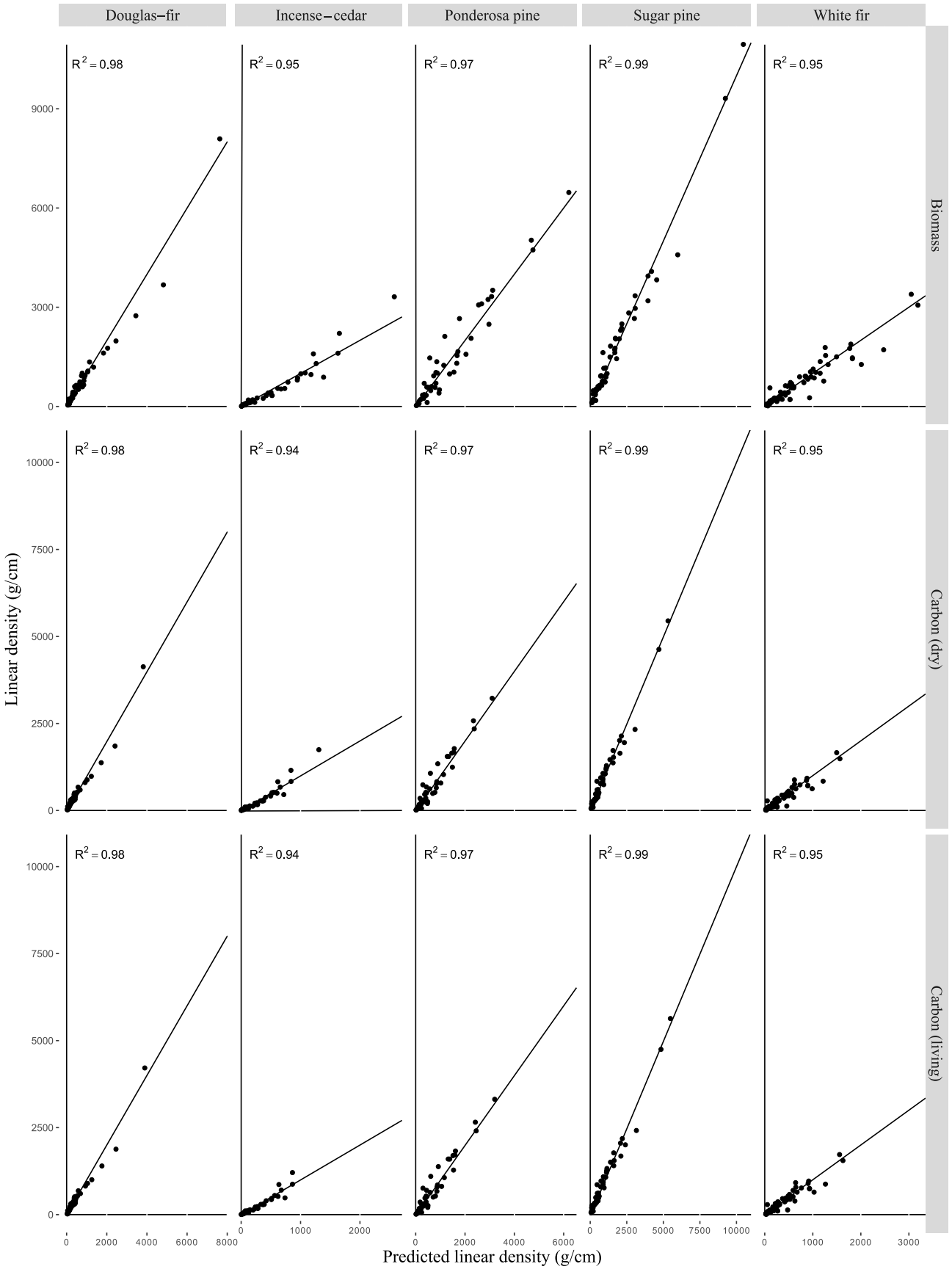

Fig. 3. Observed disk mass values versus predictions for each species and mass type. Disk mass predictions were derived by numerically integrating Model 5 from Table 3 for each species and mass type. The blue line represents the linear regression of observed mass versus predicted masses. Slope estimates for the linear regression are shown along with respective standard errors. R^2 represent the proportion of variance explained by the linear model fit.

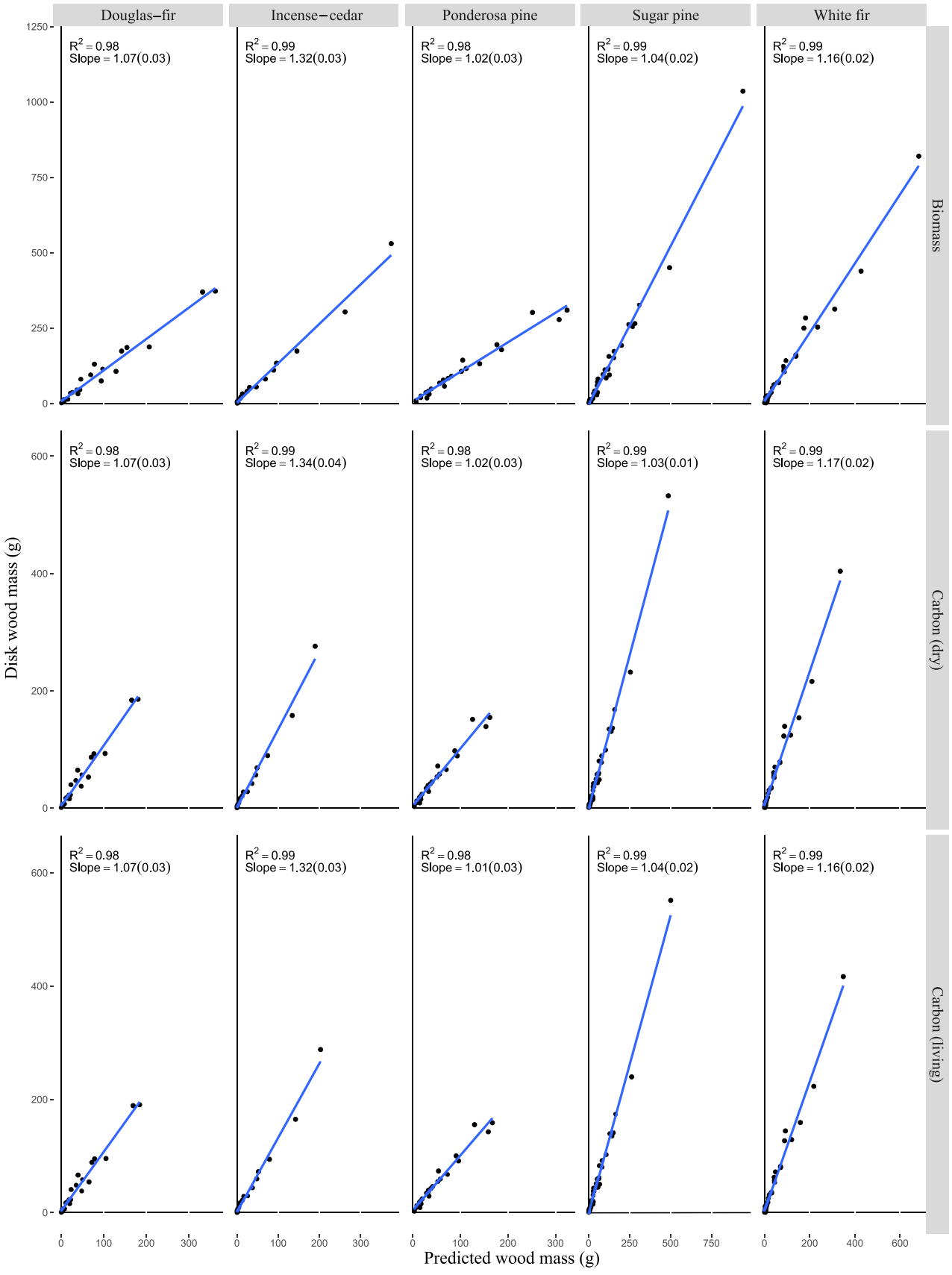

based on core data tend to underestimate the mass of the tree disks. This underestimation appears to be systematic within a species as the addition of the C_S parameter creates a relatively even distribution of data around the regression line and slope estimates are statistically identical across the mass types. There is considerable variation between the species in the Cs parameter (Table 3), potentially indicating differences in expansion of tree cores after extraction between species with the highest values found in incense-cedar.

Relationships between bark mass as a proportion of disk wood mass for biomass, oven-dry carbon, and living carbon are shown in Fig. S2. The data appear to be well-modeled using a linear fit of predicted bark mass against measured wood mass of tree disks. There is no apparent departure from the linear relationship along the spread of the data. The lowest R^2 was 0.96. The slope values shown are the parameter estimates for α_s from Model 10 (Table 3) and can be used to estimate total disk mass (M_{dt}) using eq. 1 below with M_{dw} equal to wood mass of a tree bole segment or total bole wood.

$$(1) \qquad M_{dt} = (1 + \alpha_s) \times M_{dw}$$

There was considerable variation in α_s values between species indicating differences in total bole biomass allocated to bark, with significant variation shown between mass types as well, indicating that using measured carbon fractions for tree tissues alters the overall mass balance estimates within tree boles.

Branch and foliage mass

Parameter estimates for the individual, and total tree branch mass models 8 and 9 are shown in Table S3. Individual branch mass predictions versus measurements are shown in Fig. S3, and total tree branch mass predictions versus total tree branch mass measurements are shown in Fig. S4. The random effects significantly improved the model fit for the individual branch mass models indicating that individual trees demonstrate significant differences in the modeled branch mass relationships. For tree total branch mass modeling, shown in Fig. S4, the random effects did not improve the fit of the models as demonstrated by the R_m^2 and R_c^2 values being equal.

The addition of branch height divided by total tree height, or relative height (RH), to the parameters in the individual branch models improved the overall fit, indicating that relative branch position influences mass predictions in addition to branch cross-sectional area. The influence of these additional covariates was significantly different between species as shown by the different parameter estimates reported in Table S3, for the RH covariate. Total tree branch mass models were significantly improved with the addition of live crown ratio (LCR), and height to the base of live crown (HLC) (Table S3). The model fits were improved by allowing parameter estimates for the HLC covariate to vary for each species, while leaving all other parameters fixed within a given mass type estimate. The consistency of the parameter estimates for the LCR covariate in the β_s parameter indicates the strong connection between tree size, live crown ratio and branch mass across species and mass types.

Individual branch and total tree foliage mass model parameters are given in Table S4. The R_c^2 values are higher than the R_m^2 values for individual branch foliage models indicating an improvement in model fit with random effects included (Fig. S4). The tree total foliage mass models were not improved by including random effects as shown by the equal R_c^2 and R_m^2 values in Fig. S6 despite the significance of random effects at the individual branch level. This high level of variability in random effects suggests that using parameters of individual branch biomass models outside of a given study might result in poor predictions as the set of trees sampled may not represent the population as a whole.

The addition of RH and RDC covariates to the individual branch foliage mass models significantly improved model fit. Allowing the intercept for the α_s and the parameter associated with RH in the β_s parameter (Table S4) to vary across species also significantly improved the model fit suggesting a variable response of individual branch foliage mass to relative height for the different tree species. For tree total foliage mass estimates, only the addition of LCR to the α_s parameter significantly improved model performance. Allowing the intercept of the θ_s and the parameter associated with LCR to vary across species also significantly improved the model fit (Table S4). Whole tree branch foliage models showed no improvement with the addition of random effects despite their importance to the individual branch models.

Biomass and carbon mass estimation comparisons

Mass proportions, total tissue masses, and tree total masses for example trees representing each of the mixed conifer species are presented in Fig. 4. The left half of the tree represents masses estimated for each tissue type using CRM, which used a carbon fraction of 0.5 for all tissue types, while the right half of the trees represent mass estimates based on the models and values from this study. Areas in the trees are proportional to the mass of the tissue type represented. Total tissue type mass is shown in the box next to each tissue type. For all species, the CRM resulted in a greater proportion of mass allocated to branches; this can be seen by comparing the areas for branch mass between the left and right sides of each tree. Foliar mass estimates were more consistent across species for the CRM compared to values from this study, but on average the estimates were similar between the two methods. A greater proportion of mass was found in the boles of the example trees for this study compared to CRM. Bark mass estimates were consistently lower for the CRM compared to the values from this study.

Tree carbon mass estimates for all CRM trees are 500 kg, due to the application of a carbon fraction of 0.5. Oven-dried carbon tree masses ranged from 492 kg to 529 kg, while living carbon tree masses ranged from 514 kg to 545 kg. Across species, CRM trees showed similar proportions of total biomass allocated to branches (208–223 kg) and to foliage (60–63 kg), contrasting this with values from this study ranging from 54 to 71 kg for branches and 34–84 kg for foliage, which are larger ranges than the CRM values. Higher variation was shown in the bark and bole masses for the CRM trees across

Fig. 4. Comparison of mass estimates by tissue type and species between models from this study and CRM models. Biomass, oven-dry carbon, and living carbon mass estimates for the CRM are on the left side of each example tree in yellow boxes and estimates from this study are on the right-hand side of the tree in blue boxes. The area of each tissue type shown is proportional to the respective tissues type mass proportion for the given species and mass type.

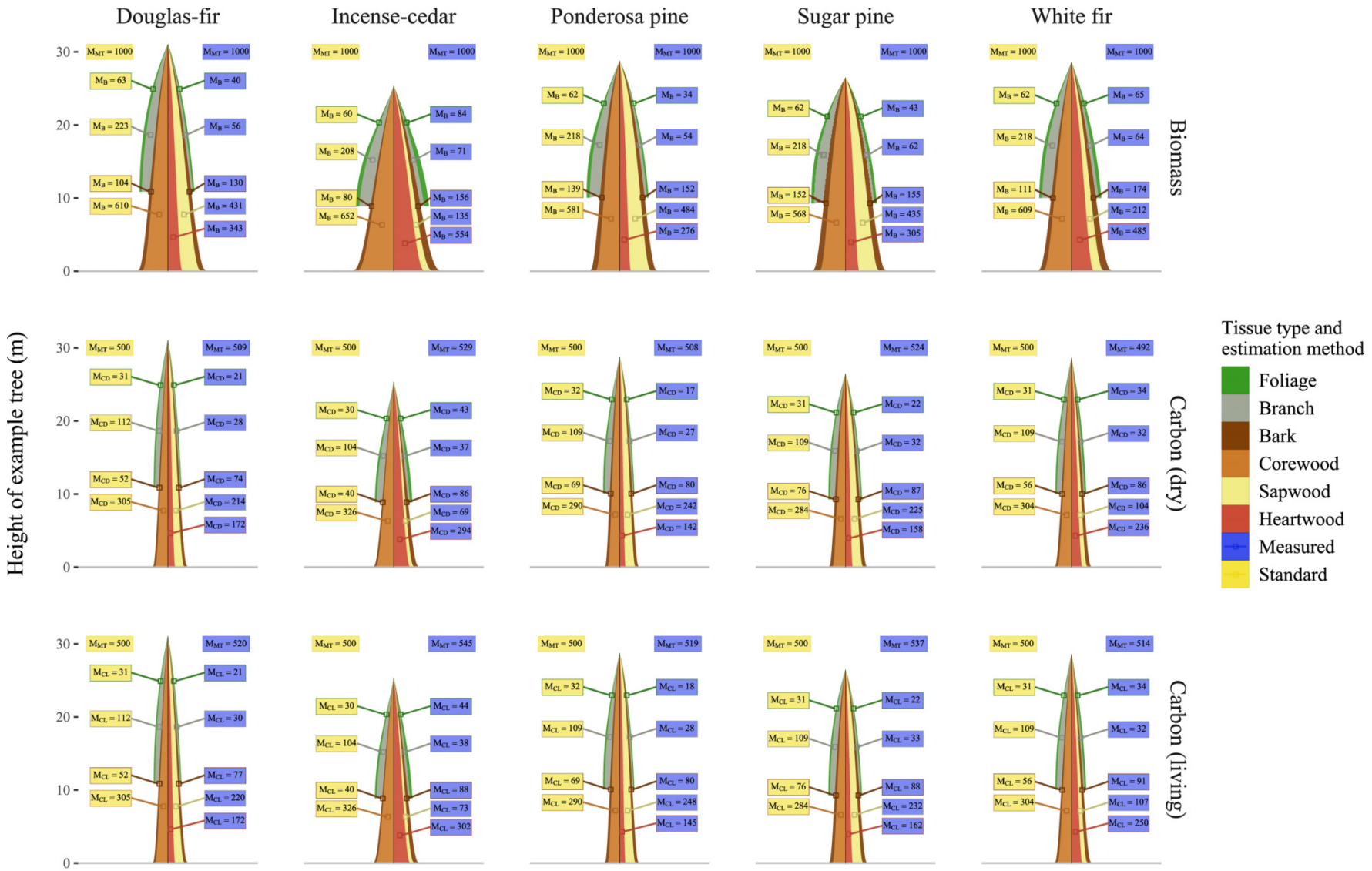

species with a range of 80–152 kg for bark and a range of 568–652 kg for bole wood. Tree mass allocated to bark and bole for this study ranged from 130 to 174 kg for bark and adding sapwood and heartwood masses together from 689 to 774 kg for bole wood. Generally, the CRM trees had less bark and bole mass than the trees from this study due to the higher proportions of mass in foliage and branch. Carbon masses show similar trends.

Discussion

Linear density

Area density was well-modeled with the approach used as shown by the tight fit of the data to the one-to-one line (Fig. S1), and R_m^2 values from 0.87 to 0.99. The final area density model fits the data significantly better than all other tested models (Table S1) after fitting additional covariates to Model 5 (Table 3). The additional covariates for each mass type and species along with parameter estimates are shown in Table S2. See Supplementary material for further discussion of area density results. By fitting Model 7 to linear density data, we have developed the first set of tree bole biomass and carbon mass prediction equations that directly account for known sources of variation within tree boles. Though other biomass functions exist that account for density variation (Zakrzewski and Duchesne 2012; Ver Planck and MacFarlane 2014), we are not aware of any carbon prediction models that account for the variation in carbon mass due to the biomass proportion of wood types. Accounting for the differences in carbon fraction shown in Table 2 is critical to creating accurate carbon mass predictions when tissue type carbon fractions vary from each other or from the widely used 0.5 carbon conversion factor.

The models developed here also produce carbon mass predictions that account for the biomass proportions of sapwood and heartwood in tree stems and stem portions. Predicting carbon mass in portions of trees is required to correctly account for carbon flow out of tree stands during timber harvesting operations, where portions of trees such as branches and treetops may be left on site while the merchantable boles are sent to a mill. Using the models presented here, tracking carbon in living trees, and in the portions of the trees that are removed, could be done with detailed stand inventory alone; this cannot be said for biomass and carbon mass models that only predict entire tree or bole masses.

Similar approaches have been used in some biomass models, but we are unaware of any model that incorporates measured carbon fraction values throughout the tree bole while also accounting for deviations in wood density and for the correlations that may exist between carbon and density (Jones and O'Hara 2018). The models presented here can be modified to include bark carbon mass by multiplying the linear density estimates by one plus the respective slopes shown in Fig. S2, which are equivalent to the α_s parameters for Model 10 (Table 3); to get calibrated values, the result of the previous step would be multiplied by the corresponding C_s value from Table 4. This allows tracking biomass and carbon mass for each tissue type found in tree boles. Given that different bole tissue types decay at different rates (Cousins et al. 2015), accurately estimating the carbon masses of tree tissue types that are left behind after timber harvest, or due to natural disturbances, would improve tracking of carbon emissions from these pools. This is especially true for species such as incense-cedar with decay-resistant heartwood that also have the highest proportion of mass allocated to that tissue of all the species in the study.

The living carbon mass models from this study help fill a gap in carbon estimates as oven-dry carbon fractions are not representative of living carbon due to the loss of volatile carbon compounds during oven-drying (Lamlom and Savidge 2003; Thomas and Martin 2012; Jones and O'Hara 2016). It therefore follows that the standard assumption of a universal 0.5 conversion factor does not accurately represent individual species. This makes our carbon models more accurate for two reasons: (1) they explicitly account for carbon in living tissues, and (2) they account for variation in carbon fraction, and density between tissue types and tree species. Using the models presented here, it is a simple matter to derive whole tree, biomass-weighted carbon fractions by dividing either of the carbon mass models for a particular tree tissue by the respective biomass model, for a given tree. These biomass-weighted carbon fractions could then be used to convert biomass estimates derived from existing biomass models for the respective species to carbon mass estimates that are more accurate than using a value of 0.5.

Disk wood mass predictions

There are several sources of potential error in developing linear density estimates from cores. The primary concern is that cores are not always representative of the density measured in disks (Williamson and Wiemann 2010). That is why calibrating the model with data from tree disks taken along tree boles is necessary. From the slopes shown in Fig. 3, which range from 1.02 to 1.32, predictions from cores consistently underestimated the disk mass values in this study, though not always significantly. This could be caused by core samples expanding along the length of the core after extraction from the tree, thereby increasing the measured volume estimate of the core segment while leaving the core segment mass unchanged, or due to higher losses of volatile material during oven-drying in the cores compared to disks due to the greater surface area to mass ratio of cores compared to disks.

The quality of the adjusted prediction values (Fig. 3) of disk mass predicted by Model 7 is surprising given the variability in individual trees shown in the core data. This helps demonstrate the viability of this approach in developing accurate prediction models inclusive of large diameter trees, an important issue in tree biomass and carbon mass estimation (Lutz et al. 2017). Additionally, these calibrated models can accurately represent the variation that occurs within tree boles. There was no increase or decrease in model predictive power along the range of disk wood masses including stump height disks, indicating that the models worked well for the entire tree bole.

Branch and foliage mass

Individual branch mass (Fig. S3), total tree branch mass (Fig. S4), individual branch foliage mass (Fig. S5), and tree to-

tal foliage mass (Fig. S6) models were the least accurate of the mass prediction models. This is somewhat expected as tree crowns are highly variable. The predictions are still reasonably good at the whole tree level with the lowest R^2 of 0.60 (Fig. S4), and an R^2 of 0.88 (Fig. S6) for ponderosa pine branch and foliage mass estimates, respectively. Though these two tree features tend to be smaller percentages of the total tree biomass and therefore have a relatively small impact on total tree carbon mass, the combination of these two masses along with treetops represent important carbon pools left on site after harvesting activities and therefore should be considered important for biomass studies.

Studies that modeled branch biomass have used a similar model form as Model 9 (Jenkins et al. 2003; Chojnacky et al. 2014), but our study allowed for modifications of this base model with the addition of covariates to the model parameters that improved model fit. The improvement in model fit with the inclusion of height to base of live crown (HLC) to the exponential component of the model is a logical result as total branch biomass should increase with tree size, and larger trees tend to have higher HLC values. The improvement in model fit with the addition of LCR is not surprising as trees with high LCR ratios and high HLC values would have long live crowns relative to total tree height. The improvement in model fit with the addition of LCR could also imply variable responses to wind force on crowns as high LCR is associated with increased wind stress on a tree. Though we allowed the LCR and α_s parameters to vary by species, there were no significant differences. This suggests a consistent exponential relationship between branch mass and LCR that is somewhat surprising given the highly variable crown structure and biomass allocations demonstrated by the species in this study.

Difference in mass proportion and total mass

There are considerable deviations in biomass proportions between our models and estimates from CRM (Fig. 4). This can be seen by comparing the two sides of each example tree while keeping in mind that each half represents a tree with a total mass of 1000 kg. Our study found higher proportions of bole wood mass and smaller proportions of branch mass compared to the CRM. It is generally understood that trees produce a given amount of carbon each year that must be allocated to the various tissue types necessary for growth, as well as cellular respiration. Understanding how that carbon is allocated has important implications for timber production as well as carbon cycling. For instance, a greater proportion of carbon in branches compared to boles would lead to more carbon left on site after harvesting. That on site material would either be burned or decay instead of being turned into wood products directly impacting carbon emission estimates related to harvest activities. Inaccuracies in biomass allocation estimates therefore have the potential to lead to suboptimal management decisions due to over- or underestimating emissions from harvesting activities, depending on which models are used.

The largest differences shown in Fig. 4 are between the CRM carbon mass estimates and the estimates using living tissue carbon fraction data. Because the example trees were each 1000 kg, these differences are due only to the proportion of biomass in a given tissue type, and the difference between using the 0.5 CRM carbon fraction and measured carbon fractions. At the whole tree carbon mass level, the differences are effectively the impact of using biomass-weighted carbon fractions for the individual tree components. In the oven-dried carbon row of Fig. 4, white fir oven-dried carbon is lower than the CRM estimate due to the lower than 0.5 carbon fraction measured for oven-dried white fir tissues. Looking directly below the oven-dried white fir tree, there is a "gain" in mass of 22 kg; this mass "gain" is due to accounting for volatile organic compounds that are lost during oven-drying. Compared to the CRM, incense-cedar living carbon is 9% higher. This value is in large part due to the allocation of mass to heartwood in that species and the higher-than-average carbon fraction for that tissue type. Similar differences due to high carbon fraction in heartwood have been found in coast redwood (Sequoia sempervirens (Lamb. Ex D. Don) Endl.) (Jones and O'hara 2012). The significance of a 9% increase in whole tree carbon mass estimates due only to correctly accounting for biomass-weighted carbon fractions cannot be understated given the extent of that species and makes a strong case for accurately measuring carbon in trees. The 2.2% to 4.5% increase in carbon mass from oven-dried to living for the other species is also important given the total biomass associated with those species; clearly, measuring living carbon fractions should be a priority for accurate carbon mass estimation.

Conclusion

This study presents stem biomass and carbon mass taper models that can be integrated to predict mass of whole boles or bole portions, along with branch and foliage prediction models, for five mixed conifer species in the Sierra Nevada. These models account for variation in carbon fraction and can be used to estimate biomass-weighted carbon fractions for the species studied. Comparisons between our models and the CRM using a standard carbon fraction of 0.5 demonstrate significant differences in carbon mass estimates as high as 9%, as well as overall biomass proportion estimates. This finding would apply equally well to any other method that relies on the 0.5 value. The models presented here allow for predictions of tree components, in addition to whole tree mass, creating the potential to track carbon on site and in harvested material with inventory data alone.

Acknowledgements

We acknowledge the assistance of Blodgett Forest manager Rob York, Southern California Edison forester Ryan Stewart, and Jackson Demonstration State Forest Research and Demonstration Program Manager Lynn Webb for assistance with locating research plots and identifying suitable sites. This work would not have been possible without the dedicated work of several field and laboratory assistants, namely Kathryn McGown, Haley Kitchens, Nico Alegria, Michelle Chen, Elizabeth Ebert, Brita Rustad, and Kate Clyatt.

Article information

History dates

Received: 8 June 2023
Accepted: 12 August 2023
Accepted manuscript online: 22 August 2023
Version of record online: 10 October 2023

Copyright

Data availability

Data generated or analyzed during this study are available from the corresponding author upon reasonable request.

Author information

Author ORCIDs

Dryw A. Jones https://orcid.org/0000-0003-0012-1067

Author notes

Author O'Hara was working as an independent researcher at the time of publication.

Author contributions

Conceptualization: DAJ
Data curation: DAJ
Formal analysis: DAJ
Funding acquisition: KLO
Investigation: DAJ
Methodology: DAJ
Project administration: DAJ
Resources: DAJ
Software: DAJ
Supervision: DAJ, KLO
Validation: DAJ
Visualization: DAJ
Writing – original draft: DAJ
Writing – review & editing: DAJ, KLO

Competing interests

The authors declare there are no competing interests.

Funding information

The authors declare no specific funding for this work.

Supplementary material

Supplementary data are available with the article at https://doi.org/10.1139/cjfr-2023-0133.

References

Ajtay, G.L., Ketner, P., and Duvigneaud, P. 1979. Terrestrial primary production and phytomass. In The Global Carbon Cycle: SCOPE 13. Wiley and Sons, Ratzeburg, Germany. p. 39.

Biging, G.S. 1984. Taper equations for second-growth mixed conifers of Northern California. For. Sci. **30**: 1103–1117.

Brown, S. 2002. Measuring carbon in forests: current status and future challenges. Environ. Pollut. Barking Essex 1987 **116**: 363–372.

Chave, J., Andalo, C., Brown, S., Cairns, M.A., Chambers, J.Q., Eamus, D., et al. 2005. Tree allometry and improved estimation of carbon stocks and balance in tropical forests. Oecologia, **145**: 87–99. doi:10.1007/s00442-005-0100-x. PMID: 15971085.

Chave, J., Coomes, D., Jansen, S., Lewis, S.L., Swenson, N.G., and Zanne, A.E. 2009. Towards a worldwide wood economics spectrum. Ecol. Lett. **12**: 351–366. doi:10.1111/j.1461-0248.2009.01285.x. PMID: 19243406.

Chojnacky, D.C., Heath, L.S., and Jenkins, J.C. 2014. Updated generalized biomass equations for North American tree species. Forestry, **87**: 129–151. doi:10.1093/forestry/cpt053.

Cohen, W.B., Harmon, M.E., Wallin, D.O., and Fiorella, M. 1996. Two decades of carbon flux from forests of the Pacific Northwest. BioScience, **46**: 836–844. doi:10.2307/1312969.

Cousins, S.J.M., Battles, J.J., Sanders, J.E., and York, R.a. 2015. Decay patterns and carbon density of standing dead trees in California mixed conifer forests. For. Ecol. Manag. **353**: 136–147. doi:10.1016/j.foreco.2015.05.030.

de Aza, C.H., Turrión, M.B., Pando, V., and Bravo, F. 2011. Carbon in heartwood, sapwood and bark along the stem profile in three Mediterranean Pinus species. Ann. For. Sci. **68**: 1067–1076. doi:10.1007/s13595-011-0122-y.

Elias, M., and Potvin, C. 2003. Assessing inter-and intra-specific variation in trunk carbon concentration for 32 neotropical tree species. Can. J. For. Res. **33**: 1039–1045. doi:10.1139/X03-018.

Eskelson, B.N.I., Monleon, V.J., and Fried, J.S. 2016. A 6 year longitudinal study of post-fire woody carbon dynamics in California's forests. Can. J. For. Res. **46**: 610–620. doi:10.1139/cjfr-2015-0375.

Fahey, T.J., Woodbury, P.B., Battles, J.J., Goodale, C.L., Hamburg, S., Ollinger, S., and Woodall, C.W. 2009. Forest carbon storage: ecology, management, and policy. Front. Ecol. Environ. **8**: 245–252. doi:10.1890/080169. PMID: 32313513.

Goodale, C.L., Apps, M.J., Birdsey, R.A., Field, C.B., Heath, L.S., Houghton, R.A., et al. 2002. Forest carbon sinks in the Northern Hemisphere. Ecol. Appl. **12**: 891–899. doi:10.1890/1051-0761(2002)012[0891:FCSITN]2.0.CO;2.

Hoover, C., and Stout, S. 2007. The carbon consequences of thinning techniques : stand structure makes a difference. J. For. **105**: 266–270.

Jenkins, J.C., Chojnacky, D.C., Heath, L.S., and Birdsey, R.A. 2003. National-scale biomass estimators for United States tree species. For. Sci. 49.

Jones, D., and O'Hara, K. 2018. Variation in carbon fraction, density, and carbon density in conifer tree tissues. Forests, **9**: 430. doi:10.3390/f9070430.

Jones, D.A., and O'Hara, K.L. 2016. The influence of preparation method on measured carbon fractions in tree tissues. Tree Physiol. **36**: 1177–1189. doi:10.1093/treephys/tpw051. PMID: 27329294.

Jones, D.A., and O'Hara, K.L. 2012. Carbon density in managed coast redwood stands: implications for forest carbon estimation. Forestry, **85**: 99–110. doi:10.1093/forestry/cpr063.

Jones, D.A., O'Hara, K.L., Battles, J.J., and Gersonde, R.F. 2015. Leaf area prediction using three alternative sampling methods for seven Sierra Nevada conifer species. Forests, **6**: 2631–2654. doi:10.3390/f6082631.

Jordan, L., Souter, R., Parresol, B., and Daniels, R.F. 2006. Application of the algebraic difference approach for developing self-referencing specific gravity and biomass equations. For. Sci. **52**: 81–92.

Lamlom, S.H., and Savidge, R.A. 2006. Carbon content variation in boles of mature sugar maple and giant sequoia. Tree Physiol. **26**: 459–468. doi:10.1093/treephys/26.4.459. PMID: 16414925.

Lamlom, S.H., and Savidge, R.A. 2003. A reassessment of carbon content in wood: variation within and between 41 North American species. Biomass Bioenergy, **25**: 381–388. doi:10.1016/S0961-9534(03)00033-3.

Langum, C.E., Yadama, V., and Lowell, E.C. 2009. Physical and mechanical properties of young-growth Douglas-Fir and Western Hemlock from Western Washington. For. Prod. J. **59**: 37–47.

Lutz, J., Matchett, J., Tarnay, L., Smith, D., Becker, K., Furniss, T., and Brooks, M. 2017. Fire and the distribution and uncertainty of carbon sequestered as aboveground tree biomass in Yosemite and Sequoia & Kings Canyon National Parks. Land, **6**: 10. doi:10.3390/land6010010.

Mattson, K.G., and Zhang, J. 2019. Forests in the northern Sierra Nevada of California, USA, store large amounts of carbon in different patterns. Ecosphere, **10**. doi:10.1002/ecs2.2778.

Melson, S., and Harmon, M. 2011. Estimates of live-tree carbon stores in the Pacific Northwest are sensitive to model selection. Carbon Balance Manag. **6**: 2. doi:10.1186/1750-0680-6-2. PMID: 21477353.

Nakagawa, S., and Schielzeth, H. 2013. A general and simple method for obtaining R2 from generalized linear mixed-effects models. Methods Ecol. Evol. **4**: 133–142. doi:10.1111/j.2041-210x.2012.00261.x.

Parresol, B.R., and Thomas, C.E. 1989. A density-integral approach to estimating stem biomass. For. Ecol. Manag. **26**: 285–297. doi:10.1016/0378-1127(89)90089-3.

Pinheiro, J., Bates, D., DebRoy, S., and Sarkar, D.,Team, R.C. 2015. nlme: linear and nonlinear mixed effects models.

Pinheiro, J., Bates, D., DebRoy, S., and Sarkar, D.R Core Team, 2019. Linear and nonlinear mixed effects models.

R Development Core Team. 2015. R: a language and environment for statistical computing.

Rueda, R., and Williamson, G.B. 1992. Radial and vertical wod specific-gravity in Ochroma pyramidale (Cav ex Lam) Urb (Bombacaceae). Biotropica, **24**: 512–518. doi:10.2307/2389013.

Soetaert, K. 2009. rootSolve: nonlinear root finding, equilibrium and steady-state analysis of ordinary differential equations.

Thomas, S.C., and Malczewski, G. 2007. Wood carbon content of tree species in Eastern China: interspecific variability and the importance of the volatile fraction. J. Environ. Manage. **85**: 659–662. doi:10.1016/j.jenvman.2006.04.022. PMID: 17187921.

Thomas, S.C., and Martin, A.R. 2012. Carbon content of tree tissues: a synthesis. Forests, **3**: 332–352. doi:10.3390/f3020332.

Ver Planck, N.R., and MacFarlane, D.W. 2014. A vertically integrated whole-tree biomass model. Trees, **29**: 449–460. doi:10.1007/s00468-014-1123-x.

Williamson, G.B., and Wiemann, M.C. 2010. Measuring wood specific gravity…correctly. Am. J. Bot. **97**: 519–524. doi:10.3732/ajb.0900243. PMID: 21622413.

Woodall, C.W., Heath, L.S., Domke, G.M., and Nichols, M.C. 2011. Methods and equations for estimating aboveground volume, biomass, and carbon for trees in the U.S. forest inventory (No. NRS-GTR-88). U.S. Department of Agriculture, Forest Service, Northern Research Station, Newtown Square, PA. doi:10.2737/NRS-GTR-88.

Woodbury, P.B., Smith, J.E., and Heath, L.S. 2007. Carbon sequestration in the U.S. forest sector from 1990 to 2010. For. Ecol. Manag. **241**: 14–27. doi:10.1016/j.foreco.2006.12.008.

Woodcock, D.W., and Shier, A.D. 2002. Wood specific gravity and its radial variations: the many ways to make a tree. Trees, **16**: 437–443. doi:10.1007/s00468-002-0173-7.

Zakrzewski, W.T., and Duchesne, I. 2012. Stem biomass model for jack pine (*Pinus banksiana Lamb.*) in Ontario. For. Ecol. Manag. **279**: 112–120. doi:10.1016/j.foreco.2012.05.012.

Zhao, D., Kane, M., Teskey, R., and Markewitz, D. 2016. Modeling aboveground biomass components and volume-to-weight conversion ratios for loblolly pine trees. For. Sci. **62**: 463–473. doi:10.5849/forsci.15-129.